ELSEVIER

Journal of Alloys and Compounds 446–447 (2007) 648–654

Journal of ALLOYS AND COMPOUNDS

www.elsevier.com/locate/jallcom

The electrochemistry and modelling of hydrogen storage materials☆

W.P. Kalisvaart[a,*], P. Vermeulen[a], A.V. Ledovskikh[a], D. Danilov[b], P.H.L. Notten[a,c]

[a] *Eindhoven University of Technology, 5600 MB Eindhoven, The Netherlands*
[b] *Eurandom, 5600 MB Eindhoven, The Netherlands*
[c] *Philips Research Laboratories, 5656 AE Eindhoven, The Netherlands*

Received 20 September 2006; accepted 9 November 2006
Available online 11 December 2006

Abstract

Mg-based alloys are promising hydrogen storage materials because of the high gravimetric energy density of MgH_2 (7.6 wt.%). A major disadvantage, however, is its very slow desorption kinetics. It has been argued that, in contrast to the well-known rutile-structured Mg hydride, hydrided Mg-transition metal alloys have a much more open crystal structure facilitating faster hydrogen transport. In this paper, the electrochemical aspects of new Mg–Sc and Mg–Ti materials will be reviewed. Storage capacities as high as 6.5 wt.% hydrogen have been reached with very favourable discharge kinetics. A theoretical description of hydrogen storage materials has also been developed by our group. A new lattice gas model is presented and successfully applied to simulate the thermodynamic properties of various hydride-forming materials. The simulation results are expressed by parameters corresponding to several energy contributions, for example mutual atomic hydrogen interaction energies. A good fit of the lattice gas model to the experimental data is found in all cases.

Keywords: Metal hydrides; Electrochemical hydrogen storage; Lattice gas model; Mg-based alloys

1. Introduction

As fossil fuels are running out, alternative ways have to be found to meet the energy demands of the future. The development of a hydrogen-driven economy may be a viable solution to the problem of possible future energy shortages [1]. However, some major technical challenges will have to be overcome, one of which is finding an efficient and safe storage medium with a small volume and low weight. Storing hydrogen in metal hydrides has the advantage of moderate operating temperatures and pressures, compared to pressurized or liquefied hydrogen, making it a serious option for mobile applications such as hybrid electric vehicles (HEVs).

The present-day AB_5-type materials that are used in Nickel-Metal Hydride (Ni-MH) batteries can only store about 1.1 wt.% H [2,3]. Because the amount of built-in functionality in portable applications, such as mobile phones and PDAs, is steadily increasing, (battery-)materials with a higher gravimetric energy density are actively sought after. Also, before hydrogen storage materials can ever be used in, for e.g., automotive applications, finding a material with a higher H-content than a mere 1 wt.% H is required.

MgH_2 has a very high reversible storage capacity of 7.6 wt.% hydrogen. A major disadvantage, however, is its very slow desorption kinetics [4] making its practical application very difficult. Therefore, ways to improve the kinetic properties by alloying Mg with another element have to be undertaken. In 1995, Huiberts et al. at the VU in Amsterdam discovered that Rare-Earth (RE) thin films can be switched from reflecting to transparent upon hydrogen exposure, going from the dihydride to the trihydride state [5,6]. Subsequently, at Philips Research, van der Sluis et al. discovered that addition of Mg to a wide variety of RE thin films improved the transparency and also achieved colour-neutrality in the fully loaded, transparent, state [7,8]. It was also established that most

☆ Invited plenary lecture MH2006.

* Corresponding author. Tel.: +31 40 2744010.
E-mail address: nlv15557@natlab.research.philips.com (W.P. Kalisvaart).

0925-8388/$ – see front matter © 2006 Elsevier B.V. All rights reserved.
doi:10.1016/j.jallcom.2006.11.031

Mg-RE thin films exhibit a highly absorbing 'black state' before becoming transparent, making them potentially useful as optical switches. The switching time between black and transparent was found to remain quite short for Mg-contents as high as 70 at.% [9]. Therefore, it could be expected that bulk Mg-RE alloys with a high magnesium content can reversibly store a large amount of hydrogen, while retaining excellent sorption kinetics.

This was shown to hold for Mg–Sc alloys, which were investigated by our group in both bulk and thin film form [10,11]. Storage capacities as high as 6.5 wt.% hydrogen with good sorption kinetics were found for alloys with a Mg-content ranging from 50 to 80 at.%. The retention of the fluorite-type crystal structure of ScH_2 was argued to be responsible for the favourable discharge kinetics compared to the rutile structure of pure MgH_2. Therefore, besides the electrochemical and thermodynamic properties, some crystallographic aspects of these alloys and their hydrides will also be reviewed in the present paper.

Because Sc is a very expensive element (~10–15 USD/g), cheaper replacements were also sought after. Because the fluorite structure, as opposed to the rutile structure of MgH_2, is believed to be crucial for obtaining favourable sorption kinetics, substituting elements were chosen from the group of elements that also form dihydrides with the fluorite structure. This, in principle, limits the choice to Ti, V, Cr, Y, Zr, Nb, La, and the rare earths, Hf and Ta. Of course, from a gravimetric energy-density point of view, 3D-transition metals are preferable. A number of these alloys have been investigated by our group in thin film form [12] and the results will also be shown here.

Recently, a lattice gas model was presented by our research group and successfully applied to various hydride-forming materials [13–15]. The model is able to accurately describe the isotherms of metal hydrides (MH) as a function of hydrogen concentration in both the α and β solid solutions and the two-phase coexistence region. The simulation results are expressed by eight parameters corresponding to several energy contributions and the normalized H-content at the phase transition points. In particular, equilibrium characteristics of $LaNi_yCu_{1.0}$ alloys with $4.0 \leq y \leq 5.0$ and MischMetal-based AB_5 compounds as a function of temperature and of Pd thin films as a function of layer thickness were simulated, and excellent agreement between calculated and experimental isotherms was observed [14,15].

In the present paper, a brief description of the model will be given together with the resulting mathematical expressions for the equilibrium electrode potential and equilibrium gas pressure. Furthermore, the model will be applied to isotherms of Mg_ySc_{1-y} thin films for several Mg-contents y, and the results will be compared with those obtained on $LaNi_4Cu$.

2. Mg–Sc bulk alloys and thin films

Mg_ySc_{1-y} alloys and thin films have been studied in the compositional range $y = 1$–0.65. It was initially argued that the alloys would store two hydrogen per Mg and three hydrogen atoms per Sc atom according to [10]:

$$Mg_ySc_{1-y} + (3-y)H_2O + (3-y)e^- \rightarrow Mg_ySc_{1-y}H_{3-y} + (3-y)OH^- \quad (1)$$

Because of the very negative heat of formation of pure ScH_2, only 1 H/Sc and 2 H/Mg were assumed to be reversible:

$$Mg_ySc_{1-y}H_{3-y} + (y+1)OH^- \leftrightarrow Mg_ySc_{1-y}H_{2-2y} + (y+1)H_2O + (y+1)e^- \quad (2)$$

To investigate whether the actual storage capacity matches these expectations, electrochemical measurements were carried out on thin films and bulk alloys. All electrochemical experiments are carried out at room temperature. The preparation of both the thin films and bulk alloys/electrodes has been extensively described elsewhere [11], together with the experimental setup. Fig. 1 shows the initial constant-current (CC) charge and discharge of a bulk $Mg_{0.65}Sc_{0.35}Pd_{0.024}$ alloy. Charging was done with a current density of 250 mA/g (curve (a)), discharging was performed at a rate of 50 mA/g (curve (b)) followed by a deep-discharge at 10 mA/g (curve (c)).

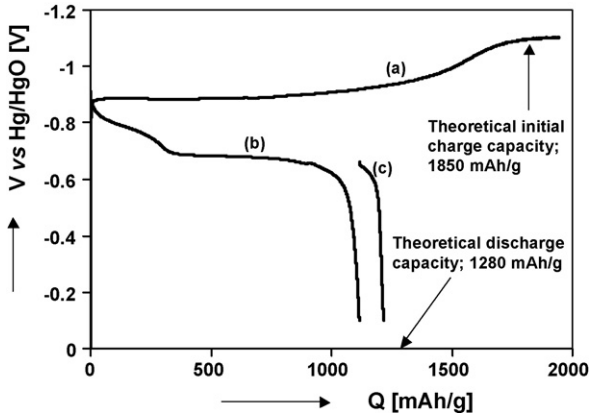

Fig. 1. Galvanostatic charge and discharge curve of a bulk $Mg_{0.65}Sc_{0.35}Pd_{0.024}$ alloy. Charging was done at a current density of 250 mA/g, discharging at 50 mA/g followed by 10 mA/g. Theoretically expected charge and discharge capacities are also indicated.

According to Eq. (1), the initial charge capacity for this composition should be 1850 mAh/g, which is indeed the case as can be seen in Fig. 1. Despite the oversimplification of the charging behaviour; pure ScH_2 absorbs a third H-atom only at extremely high pressures [16], the experimental findings correspond very well with the expectations. Apparently, since the molar volume of MgH_2 is about 10% larger than that of ScH_2, the expansion of the hydrided material with respect to pure ScH_2 allows the third hydrogen atom to be absorbed at ambient conditions. The expected discharge capacity for $y = 0.65$ according to Eq. (2) is 1280 mAh/g, which is also almost reached as can be seen in Fig. 1.

Fig. 2 depicts the constant-current discharge curves for Mg_ySc_{1-y} thin films (a) and bulk alloys (b). In Fig. 2, it can be seen that the electrochemical properties of thin films and bulk materials strongly resemble each other. After an initial solid-solution region, a very broad plateau can be seen for com-

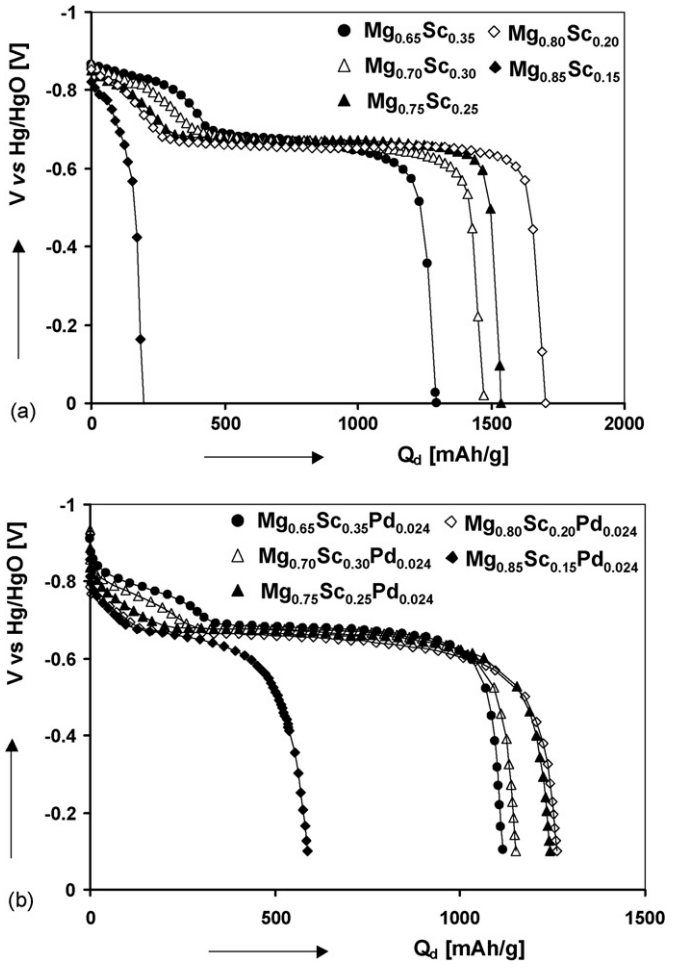

Fig. 2. Galvanostatic discharge curves of 200 nm thick Pd-capped Mg_xSc_{1-x} thin films (a), and Pd-doped bulk materials (b); the current density was 1000 mA/g for the thin films and 50 mA/g for the bulk materials.

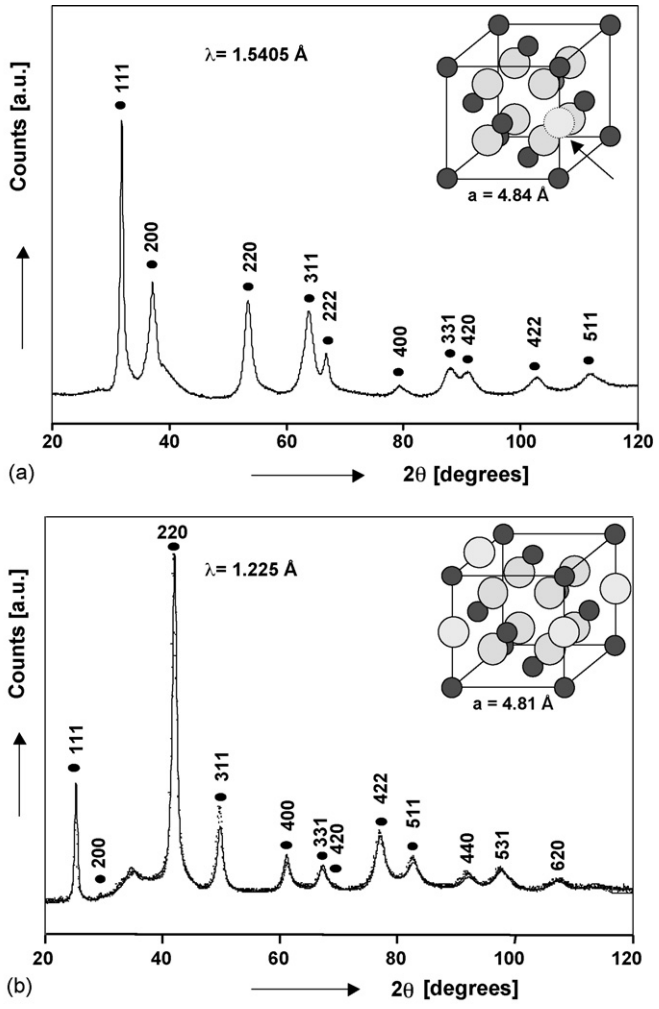

Fig. 3. X-ray diffractogram of bulk hydrided $Mg_{0.65}Sc_{0.35}Pd_{0.024}$ (a), and neutron diffractogram of deuterated $Mg_{0.65}Sc_{0.35}Pd_{0.024}$ (b). Wavelengths, lattice constants, and Miller indices are also shown, together with a graphical representation of the unit cell.

positions $x = 0.65$ to 0.80, which is indicative of a two-phase co-existence. The plateau ranges from hydrogen contents of approximately 2 H/M to 1 H/M. The plateau voltage is virtually independent of composition and is about –0.68 V versus Hg/HgO. The same is true for the equilibrium voltage curves, which look essentially the same as the CC-curves and show a plateau voltage at –0.73 V, which can be converted to a partial hydrogen pressure according to:

$$E_{eq} = -\frac{RT}{n\mathrm{F}} \ln \frac{P_{H_2}}{P_0} - 0.931 \quad (3)$$

where R is the gas constant, F is Faraday's constant and P_0 is the standard pressure of 1 bar. An equilibrium voltage of –0.73 V then corresponds to a plateau pressure of about 10^{-7} bar [11].

As can be seen in Fig. 2, the discharge capacity first increases going from $y = 0.65$–0.80. This is to be expected since increasing the Mg-content makes the material lighter, thereby increasing the gravimetric storage capacity. However, beyond $y = 0.80$, a sharp decline in capacity is observed. This has been attributed to a change in the crystal structure from fluorite to rutile, which is known to act as a blocking layer for hydrogen diffusion [17].

For composition $y = 0.65$, the crystal structure of the hydrided material has been studied with both X-ray and neutron diffraction [18]. The X-ray diffractogram of a fully hydrided and the neutron diffractogram of a fully deuterated $Mg_{0.65}Sc_{0.35}Pd_{0.024}$ alloy are shown in Fig. 3. It can be seen from the X-ray diffractogram (Fig. 3a) that the FCC structure of the metal sublattice of ScH_2 is retained in the ternary hydride. The lattice constant (4.84 Å) is larger than for pure ScH_2 (4.78 Å), which means that a ternary hydride has indeed been formed.

The fully hydrogen-loaded materials have a fluorite structure, which is also shown in Fig. 3 in the top right corner. At H(D)/M = 2, all tetrahedral sites in the crystal lattice are filled, which is indicated by the solid light-gray spheres. An empty octahedral interstitial is indicated with the arrow. It is the presence of these large empty interstices that is believed to enable rapid hydrogen diffusion compared to rutile MgH_2.

However, it was determined by chemical analysis that the fully charged hydride contains 2.25 H/M, which means that besides the tetrahedral sites, the octahedral sites must be partly occupied as well. Because XRD does not show where the hydro-

gen atoms are located, a fully deuterated material was subjected to neutron diffraction analysis (Fig. 3b). From the diffraction pattern, a T-site occupancy of 2 D/M and an O-site occupancy of 0.25 D/M can be derived, verifying the partial filling of the octahedral sites.

The phase transition occurring in the plateau region of the discharge curves was also studied. Partial desorption of both the hydride and deuteride showed co-existence of 2 FCC phases with different H(D)-site occupancies and lattice constants [11,18]. The discrete expansion associated with the phase transition turned out to be well below 10%, much lower than for example $LaNi_5$ (21%), which is favourable for the cycling stability of the material.

3. Mg-TM thin films

Although Mg–Sc alloys are quite promising with regard to the high energy density and the low discrete expansion, the high cost of Sc makes practical application unlikely. Therefore, other Mg-Transition Metal combinations were also investigated. From earlier work performed at AIST, Osaka University, and the Ahrrenius laboratory in Stockholm, it was already known that small quantities of a number of Mg-rich Mg-TM hydrides can be synthesized at ultra-high pressures. Mg_3MnH_6, Mg_3CrH_6, Mg_6VH_x, $Mg_7TiH_{\sim 13}$ [19–22] and more recently $Mg_{6.5}NbH_{\sim 14}$ [23] were synthesized using an anvil-cell technique. Of this series of novel hydrides, only Mg_6VH_x and $Mg_7TiH_{\sim 13}$ were found to have the same face-centered cubic structure as $Mg_{0.65}Sc_{0.35}H_{2.3}$.

The above-mentioned group of hydrides was synthesized from MgH_2 and the appropriate transition-metal(hydride), with an internal hydrogen source such as $NaBH_4$ [21] at high temperatures. Also, desorption of the hydrogen was performed at high temperatures and the reversibility of the absorption/desorption processes was not tested, which is of course the real challenge in finding a viable material for rechargeable batteries or on-board hydrogen storage applications. Therefore, an attempt had to be made to synthesize these materials from the metals, preferably at or near room temperature.

Niessen and Notten investigated Mg–Ti, Mg–V and Mg–Cr thin films produced by e-beam deposition [12]. Fig. 4 depicts the high-and low-rate electrochemical dischargeability of the $Mg_{0.80}TM_{0.20}$ thin films at room temperature. Mg–Ti and Mg–V are comparable to Mg–Sc in total storage capacity, whereas Mg–Cr performs slightly worse. However, only $Mg_{0.80}Ti_{0.20}$ performs about equally well in rate capability (black bars in Fig. 4) compared to $Mg_{0.80}Sc_{0.20}$. Borsa et al. studied the optical properties of thin crystalline Mg–Ti layers and it was found that Mg–Ti also shows a highly absorbing black state, similar to Mg-RE switchable mirrors [24]. Vermeulen et al. conducted a more elaborate electrochemical study of the Mg–Ti system; i.e. as a function of Mg/Ti ratio [25,26]. It turned out that the discharge capacity at room temperature showed a dependence on the Mg/Ti ratio that was strongly similar to the Mg–Sc system. The optimum composition was $Mg_{0.80}Ti_{0.20}$ with a total discharge capacity of 1750 mAh/g (6.5 wt.% H) [25].

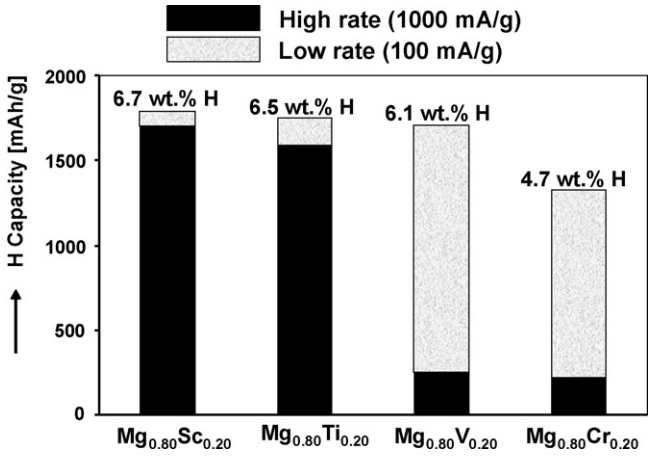

Fig. 4. Storage capacity at high (1000 mA/g) and low (100 mA/g) current density for Mg_xTM_{1-x} (TM = Sc, Ti, V, Cr) thin films.

Fig. 5a shows the first galvanostatic charging curves of Pd-capped Mg_yTi_{1-y} thin films for $y = 0.50$–0.95. Three distinct regions can be seen in the charging curves: a small plateau at more positive voltages followed by a longer sloping plateau and eventually the hydrogen-evolution reaction. The amount of hydrogen that is inserted during the first stage increases with

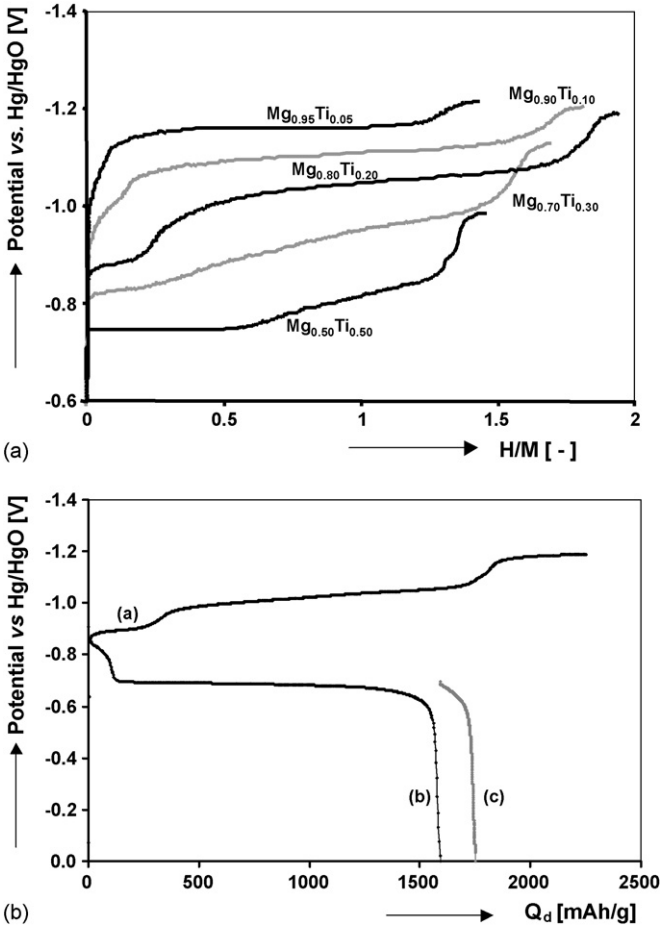

Fig. 5. (a) Galvanostatic charging curves (5 A/g) of 200 nm thick Mg_xTi_{1-x} thin films and (b) galvanostatic charge (curve (a)), discharge (1000 mA/g, curve (b)) and deep discharge (100 mA/g, curve (c)) of $Mg_{0.80}Ti_{0.20}$ (b).

increasing Ti-content. However, the voltage level of this plateau is strongly influenced by the Mg/Ti ratio, which means it is quite reasonable to assume that the Ti is surrounded by both hydrogen and Mg and that the Mg–Ti alloys also form a ternary hydride, similar to Mg–Sc. The H/M ratio that is reached during charging before the onset of the hydrogen evolution reaction is always below (or very close to) two. Contrary to Sc, the valence of Ti does not seem to exceed two, even though Ti can also be tri-or tetra-valent. This is also apparent from the galvanostatic discharge curve, which shows a much narrower solid solution region before the onset of the discharge plateau (Fig. 5b) compared to $Mg_{0.80}Sc_{0.20}$ (Fig. 2a). The voltage level is also around –0.68 V versus Hg/HgO in the middle of the plateau, the same as for Mg–Sc.

Synthesising a bulk Mg–Ti alloy that can be reversibly hydrided at room temperature is proving to be quite a challenge. In thermodynamic equilibrium, Mg and Ti have a mutual solid solubility of less than 1 at.% even at elevated temperatures and the fact that the boiling point of Mg (1090 °C) is way below the melting point of Ti (1668 °C) rules out, for example melt-spinning or other rapid-solidification routes to try and make these materials. Some successes in extending the solid solubility of Mg in Ti and vice versa by mechanical alloying have been reported [27–29]. Only Liang and Schulz have subjected the resulting material, a 12.5 at.% solid solution of Ti in Mg, to hydrogen gas at elevated temperatures, which resulted in decomposition into the binary hydrides [29].

Within our group, some interesting results have been obtained by mechanical alloying of Mg and Ti with small amounts of other metals and a Pd catalyst. The starting mixture is completely converted into two cubic compounds and can reversibly store about one third of the capacity reached with the thin films at room temperature. The results will be reported shortly in a separate paper [30].

4. Modelling of hydrogen storage materials: lattice gas model

Combining structural assumptions, mean field approximations and a binary alloy approach, our lattice gas model is able to describe the equilibrium potential of hydride-forming materials (E^{eq}_{MH}) and equilibrium pressure (P^{eq}_{MH}) as explicit functions of the normalized hydrogen concentration (x). A maximum of eight parameters is used to simulate the experimental data. These parameters are the phase-transition points (x_α and x_β), the energies of the individual hydrogen atoms in their separate phases (E_α and E_β), the H–H interaction energies within the α and β phases ($U_{\alpha\alpha}$ and $U_{\beta\beta}$), the H–H inter-phase interaction energy between hydrogen atoms located in different phases ($U_{\alpha\beta}$) and finally the energy of the host lattice (L) which corresponds to the energy of the unit cell of the hydride-forming material. Thus, according to the lattice gas model, the total description of the equilibrium potential and equilibrium pressure consists of three parts: the α- and β-solid solutions and that of the two-phase coexistence region [14–15]:

$$E^{eq}_{MH} = \frac{RT}{F}\begin{cases} \ln\left(\dfrac{1-xd}{xd}\right) - \dfrac{F}{RT}(E_\alpha + U_{\alpha\alpha}x), & 0 \le x < x_\alpha \\ \dfrac{\left(\dfrac{S^0_\alpha}{d} - S^0_\beta\right) - \dfrac{F}{RT}\left\{-E_\alpha x_\alpha - U_{\alpha\alpha}x^2_\alpha x_2 + E_\beta x_\beta + U_{\beta\beta}x^2_\beta x_1 + \dfrac{U_{\alpha\beta}x_\alpha x_\beta}{2}(x_2 - x_1) + L\right\}}{x_\beta - x_\alpha}, & x_\alpha \le x < x_\beta \\ \ln\left(\dfrac{1-x}{x}\right) - \dfrac{F}{RT}(E_\beta + U_{\beta\beta}x), & x \le x_\beta \end{cases} \quad (4)$$

$$P_{H_2} = P_{ref}\exp\frac{2F}{RT}\begin{cases} E_\alpha + U_{\alpha\alpha}x - \dfrac{RT}{F}\ln\left(\dfrac{1-xd}{xd}\right), & 0 \le x < x_\alpha \\ \dfrac{-E_\alpha x_\alpha - U_{\alpha\alpha}x^2_\alpha x_2 + E_\beta x_\beta + U_{\beta\beta}x^2_\beta x_1 + \dfrac{U_{\alpha\beta}x_\alpha x_\beta}{2}(x_2 - x_1) + L - \dfrac{RT}{F}\left(\dfrac{S^0_\alpha}{d} - S^0_\beta\right)}{x_\beta - x_\alpha}, & x_\alpha \le x < x_\beta \\ E_\beta + U_{\beta\beta}x - \dfrac{RT}{F}\ln\left(\dfrac{1-x}{x}\right), & x \le x_\beta \end{cases} \quad (5)$$

where $x_1 = (x - x_\alpha)/(x_\beta - x_\alpha)$, $x_2 = (x_\beta - x)/(x_\beta - x_\alpha)$, P_{ref} is the reference pressure of 1 bar $\cong 10^5$ Pa, R is the gas constant, T the absolute temperature and F is the Faraday constant. The entropy terms are defined as:

$$\begin{aligned} S^0_\alpha &= x_\alpha d\ \ln\ x_\alpha d + (1 - x_\alpha d)\ln(1 - x_\alpha d) \\ S^0_\beta &= x_\beta\ \ln\ x_\beta + (1 - x_\beta)\ln(1 - x_\beta) \end{aligned} \quad (6)$$

where d is the ratio between the number of host sites per unit cell in the α and β phase.

As was already stated, our model has been applied very successfully to experimental isotherms of AB_5-type materials as a function of temperature [14]. Using the same set of parameters, the thermodynamic behaviour of very thin Pd layers as a function of layer thickness can also be simulated. In 1986, Nicolas et al. showed that the critical temperature of Pd was dependent on the film thickness in the range between 6 and 60 nm [31]. Vermeulen et al. measured the isotherms of Pd films of 10–200 nm thickness electrochemically and the results were fitted with our

Table 1
Values of the fitting parameters obtained on Mg_ySc_{1-y} isotherms for $1-y=0.15$–0.35, and on $LaNi_4Cu$ using our lattice gas model

Sc content	x_α	x_β	E_α (eV)	E_β (eV)	$U_{\alpha\alpha}$ (eV)	$U_{\beta\beta}$ (eV)	$U_{\alpha\beta}$ (eV)	L (eV)
0.15	0.110	0.880	−0.154	−0.876	0.101	0.721	5.727	0.327
0.20	0.119	0.736	−0.180	−0.627	0.237	0.562	3.388	0.174
0.25	0.162	0.698	−0.212	−0.540	0.275	0.476	2.008	0.128
0.30	0.166	0.679	−0.206	−0.471	0.198	0.396	1.523	0.100
0.35	0.229	0.478	−0.213	−0.321	0.076	0.269	0.525	0.028
$LaNi_4Cu$	0.196	0.794	0.069	0.011	−0.158	−0.053	−0.257	0.020

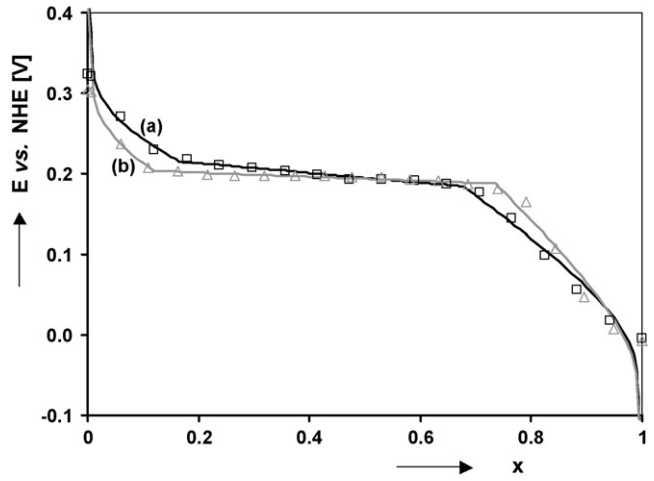

Fig. 6. Experimental isotherms (open symbols) and model fit (solid lines) of $Mg_{0.70}Sc_{0.30}$ (curve (a)) and $Mg_{0.80}Sc_{0.20}$ (curve (b)) thin films.

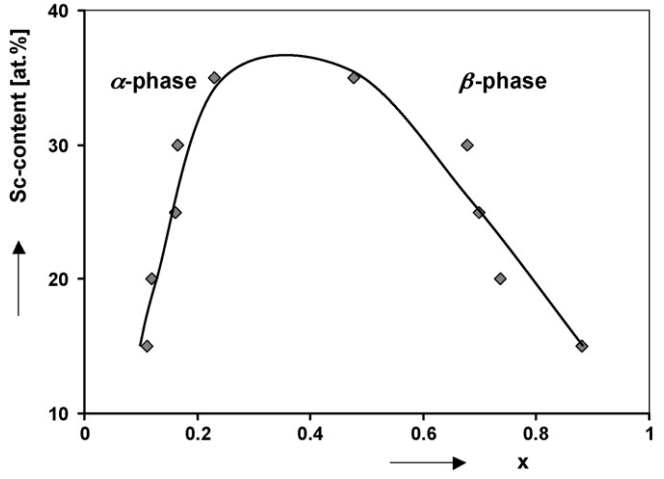

Fig. 7. Phase diagram as a function of Sc content and normalized hydrogen concentration of Mg_ySc_{1-y} thin films, as determined by our lattice gas model.

lattice gas model. Again, excellent agreement between model and experiment was observed and the miscibility gap did indeed disappear at room temperature at a layer thickness of 10 nm, evidenced by the fact that the best fit was obtained with the same value for x_α and x_β [15].

Here, we present results on the simulation of desorption isotherms of Mg_ySc_{1-y} thin films described in the previous sections. From both ND and XRD measurements on bulk hydrided Mg–Sc alloys [11,18] it is known that the α and β phase are both cubic differing only in lattice parameter and thus have the same total number of available host sites. Therefore, d was set to unity in all simulations.

The experimental equilibrium potentials (symbols) of the different compositions of Mg_ySc_{1-y} thin films (i.e. $y=0.80$ and $y=0.70$) are plotted as a function of the normalized hydrogen content together with the isotherms simulated by the lattice gas model (solid lines) in Fig. 6. One can observe a good fit of the simulation results to the experimental data, in particular in the plateau region and α-solid solution. The calculated values of all eight parameters are shown for Mg_ySc_{1-y} with $y=0.65-0.85$ together with the values obtained for $LaNi_4Cu$ [14] in Table 1.

We can very well observe that the Mg-based and AB_5-type hydrides are completely different kinds of materials. Mg_ySc_{1-y} has a much higher hydrogen affinity than $LaNi_4Cu$, which is reflected experimentally by the lower equilibrium pressure and in our model by the negative values for E_i for all Mg–Sc compositions, while for $LaNi_4Cu$ it is positive. Mg is much more electropositive than Ni or Cu, which means the resulting hydride is probably much more ionic in character. Therefore, the hydrogen atoms will have a small negative charge ($H^{\delta-}$) in the Mg-based hydrides, resulting in a repulsive intra-and interphase interaction. This is indeed reflected by positive values for $U_{\alpha\alpha}$, $U_{\beta\beta}$ and $U_{\alpha\beta}$ in the case of the Mg_ySc_{1-y} materials, whereas for $LaNi_4Cu$ these values are negative. This once more underlines the physical meaningfulness and general applicability of our model.

As the phase-transition points (x_α and x_β) are accurately determined using the mathematical model, it is possible to construct a phase diagram as a function of Sc content and normalized hydrogen concentration in the alloy. This is depicted in Fig. 7. For Sc-contents above 0.30, the phase boundaries x_α and x_β converge sharply towards a single phase-transition point as the Sc content in the alloy increases. At Sc contents slightly above 35 at.%, the miscibility gap will probably completely vanish.

5. Conclusions and outlook

Mg_ySc_{1-y} and Mg_yTi_{1-y} are both very promising materials for future hydrogen storage applications. Their kinetic properties are much more favourable compared to pure MgH_2, most likely owing to the cubic structure of the hydride as opposed to the rutile structure of MgH_2. For Mg–Sc alloys, the crystal structure has been extensively studied and a cubic fluorite structure was confirmed by both XRD and ND measurements. Partial desorption showed that the cubic structure was preserved in the

hydrogen-poor phase. Similar measurements on Mg–Ti alloys have not yet been carried out, but from the work using ultra-high pressure techniques it is known that cubic hydrides can be formed in this system as well. Efforts to make a bulk analogue of Mg–Ti, as was done for Mg–Sc, is in progress [30].

A new lattice gas model was presented and successfully applied to simulate the thermodynamics of various hydride-forming materials. An excellent fit of the lattice gas model to the experimental data was found and the corresponding parameters were used to describe several thermodynamic properties. The phase diagram of Mg_ySc_{1-y} alloy as a function of Sc content is determined and reveals that the miscibility gap completely vanishes if the Sc content exceeds 35%. The successful application of the lattice gas model to two such completely different types of materials, i.e. Mg_ySc_{1-y} and $LaNi_4Cu$, where the values of the fitting parameters precisely reflect the experimental findings shows how physically meaningful and generally applicable our model is. An extension of the model to multi-plateau isotherms and a description of hysteresis phenomena within the same lattice-gas framework are currently under way within our group.

Acknowledgements

The authors wish to express their gratitude to T. Raaymakers, J. van Laarhoven and T. Dao for thin film preparation and characterization. H. Wondergem and M. Latroche are acknowledged for XRD and neutron diffraction analysis, respectively. The group of Professor Dr. Ronald Griessen at the VU in Amsterdam is acknowledged for a fruitful collaboration on the subject of Mg–Ti thin films.

This research was performed as part of the Sustainable Hydrogen Program of Advanced Chemical Technologies for Sustainability (ACTS).

References

[1] L. Schlapbach, A. Züttel, Nature 414 (2001) 353–358.
[2] H. Senoh, K. Morimoto, H. Inoue, C. Iwakura, P.H.L. Notten, J. Electrochem. Soc. 124 (2000) 2451.
[3] J.J.G. Willems, Philips J. Res. Suppl. 39 (1984) 1.
[4] A. Zaluska, L. Zaluski, J.O. Ström Olsen, J. Alloys Compd. 288 (1999) 217–225.
[5] J.N. Huiberts, R. Griessen, J.H. Rector, R.J. Wijngaarden, J.P. Dekker, D.G. de Groot, N.J. Koeman, Nature 380 (1996) 231–234.
[6] P.H.L. Notten, M. Kremers, R. Griessen, J. Electrochem. Soc. 143 (1996) 3348.
[7] P. van der Sluis, M. Ouwerkerk, P.A. Duine, Appl. Phys. Lett. 70 (1997) 3356.
[8] P.H.L. Notten, Curr. Opin. Solid State Mater. Sci. 4 (1999) 5–10.
[9] M. Ouwerkerk, Solid State Ionics 431 (1998) 113–115.
[10] P.H.L. Notten, M. Ouwerkerk, H. van Hal, D. Beelen, W. Keur, J. Zhou, H. Feil, J. Power Sources 129 (2003) 45.
[11] W.P. Kalisvaart, R.A.H. Niessen, P.H.L. Notten, J. Alloys Compd. 417 (2006) 280–291.
[12] R.A.H. Niessen, P.H.L. Notten, Electrochem. Solid State Lett. 8 (2005) A534–A538.
[13] A. Ledovskikh, E. Verbitskiy, A. Ayeb, P.H.L. Notten, J. Alloys Compd. 742 (2003) 356–357.
[14] A. Ledovskikh, D. Danilov, W.J.J. Rey, P.H.L. Notten, Phys. Rev. Lett. B73 (2006), 014106.
[15] P. Vermeulen, A. Ledovskikh, D. Danilov, P.H.L. Notten, J. Phys. Chem. B 110 (2006) 20350.
[16] I.O. Bashkin, E.G. Ponyatovski, M.E. Kost, Phys. Status Solidi B 87 (1978) 369.
[17] B. Vigeholm, K. Jensen, B. Larsen, A. Schrøder Pedersen, J. Less Common Met. 131 (1987) 133.
[18] M. Latroche, W.P. Kalisvaart, P.H.L. Notten, J. Solid State Chem. 179 (2006) 3024–3032.
[19] H. Blomqvist, E. Rönnebro, D. Kyoi, T. Sakai, D. Noréus, J. Alloys Compd. 358 (2003) 82–86.
[20] E. Rönnebro, D. Kyoi, H. Blomqvist, D. Noréus, T. Sakai, J. Alloys Compd. 368 (2004) 279–282.
[21] D. Kyoi, T. Sato, E. Rönnebro, Y. Tsuji, N. Kitamura, A. Ueda, M. Ito, S. Katsuyama, S. Hara, D. Noréus, T. Sakai, J. Alloys Compd. 375 (2004) 253–258.
[22] D. Kyoi, T. Sato, E. Rönnebro, N. Kitamura, A. Ueda, M. Ito, S. Katsuyama, S. Hara, D. Noréus, T. Sakai, J. Alloys Compd. 372 (2004) 213–217.
[23] T. Sato, D. Kyoi, E. Rönnebro, N. Kitamura, T. Sakai, D. Noréus, J. Alloys Compd. 417 (2006) 230–234.
[24] D.M. Borsa, A. Baldi, M. Pasturel, H. Schreuders, B. Dam, P. Vermeulen, P.H.L. Notten, R. Griessen, Appl. Phys. Lett. 88 (2006), 241910.
[25] P. Vermeulen, R.A.H. Niessen, P.H.L. Notten, Electrochem. Commun. 8 (2005) 27–32.
[26] P. Vermeulen, R.A.H. Niessen, D.M. Borsa, B. Dam, R. Griessen, P.H.L. Notten, Electrochem. Solid State Lett. 9 (2006) A520.
[27] D.M.J. Wilkes, P.S. Goodwin, C.M. Ward-Close, K. Bagnall, J. Steeds, Mater. Lett. 27 (1996) 47–52.
[28] F. Sun, F.H. Froes, J. Alloys Compd. 340 (2002) 220–225.
[29] G. Liang, R. Schulz, J. Mater. Sci. Lett. 38 (2003) 1179–1184.
[30] W.P. Kalisvaart, H.J. Wondergem, F. Bakker, P.H.L. Notten, J. Mat. Res., submitted for publication.
[31] M. Nicolas, L. Dumoulin, J.P. Burger, J. Appl. Phys. 60 (1986) 3125–3130.